Perfluorodecalin to enhance reactive species delivery in plasma-biomaterial interactions

To cite this article: Daniel T Elg and David B Graves 2019 *J. Phys. D: Appl. Phys.* **52** 355204

Perfluorodecalin to Enhance Reactive Species Delivery in Plasma-Biomaterial Interactions

Daniel T. Elg[1] and David B. Graves[2]
[1]University of Southern Indiana, Department of Engineering, Evansville, IN USA
[2]University of California - Berkeley, Department of Chemical & Biomolecular Engineering, Berkeley, CA USA

Abstract. Treatment of biological tissue by non-thermal atmospheric pressure plasmas in air can often cause beneficial biological outcomes, commonly by generation and delivery of reactive oxygen and nitrogen species (RONS). Biological plasma treatment is often mediated through plasma-liquid interactions, wherein plasma-generated RONS are dissolved into the liquid phase and subsequently initiate liquid-phase chemistry. In this paper we report observations on plasma-liquid interactions using a biologically inert perfluorocarbon solvent - perfluorodecalin (PFD) - that is known to be useful in other biomedical applications. The present paper concerns thin films of liquid PFD applied to porous and non-porous surfaces and subsequent plasma exposure of these films. With PFD application as a thin film prior to plasma exposure, we observe evidence of delayed, but ultimately enhanced RONS delivery to non-porous surfaces and through porous underlying surfaces. We demonstrate that PFD dissolves and retains relatively high concentrations of plasma-produced RONS, especially NO_2. When the thin liquid film of PFD evaporates during plasma exposure, there appears to be a relatively rapid release of dissolved RONS, potentially aiding certain applications.

Keywords: Atmospheric Pressure Plasma, Plasma Medicine, RONS, plasma-liquid interactions, perfluorodecalin

Address all correspondence to: David Graves, graves@berkeley.edu

1 Introduction

Non-thermal plasma-material interactions have historically been centered on applications at low pressure. However, atmospheric pressure plasmas have become the subject of significantly increased research activity within the past decade [1]. Operation at atmospheric pressure enables many surface treatment applications that are difficult or not feasible in a vacuum environment. If the atmospheric pressure plasma species interacting with tissue or cells remains non-thermal, it is possible to safely treat biological surfaces with plasmas or their products. This field is known as plasma biomedicine. Many beneficial effects of plasma biomedicine have been reported, such as antibacterial activity, antifungal effects, wound healing, and tumor shrinkage, among others [2]–[4]. Plasmas generate many different neutral and ionic species, as well as photons, heat, electric fields, and electric currents. However, it is generally thought that many of the beneficial biological

effects seen in plasma biomedicine are caused primarily by plasma-produced reactive oxygen and nitrogen species (RONS), either directly or through liquid phase biochemistry initiated by plasma-produced RONS. RONS are known to be used throughout aerobic biology as signaling agents and in various immune system functions, in addition to other roles, so it is perhaps not surprising that they could provide beneficial effects when produced and applied externally. Identifying and rationalizing the mechanisms of non-thermal plasma-biological system interactions are topics of intense current study [5]–[8].

Plasma treatment is generally a surface-based technique but plasma biomedicine appears to generate effects beneath surfaces and in some cases beyond the expected diffusion distances of the most reactive RONS, such as OH. It is well known that living tissue contains significant quantities of water. Thus, biological effects of plasmas may be limited and mediated through plasma-liquid interactions, which determine the solvation of plasma-produced species near the surface. This solvation affects both biological effects at the surface and the ensuing chemistry deeper in the tissue. Solvation of plasma-produced species has even been reported to enhance delivery of RONS in a previously dry system under certain conditions [9]. The multiple, complex scientific issues associated with plasma-liquid interactions has recently been reviewed [10].

Most research in the field of plasma-liquid interactions has focused on the use of water as the liquid-phase. However, some applications could potentially be aided or improved by the use of a different solvent. One such solvent is perfluorodecalin (PFD), a fluorocarbon with the formula $C_{10}F_{18}$. PFD is nontoxic and has been used in other biological applications. PFD is most known for its ability to dissolve relatively high concentrations of oxygen relative to, for example, water

and other hydrophilic solvents. Much of the previous research on applications of PFD has centered on liquid ventilation and artificial blood [11]–[14].

Previously, our group reported the treatment of onychomycosis (toenail fungus) by plasma, in which the antifungal effect of the plasma was observed by measuring log reductions of *T. rubrum* toenail fungus even on the side of the nail not in direct contact with the plasma effluent [15]. Recently, clinical studies have shown that a similar technique can result in a significantly improved antifungal effect when an infected toenail to be plasma-treated is coated with PFD prior to plasma treatment [16]. The enhanced solubility of gas-phase species by PFD [17] appears to be a likely cause, but the mechanism(s) of plasma treatment enhancement by PFD has apparently not been investigated and reported.

Despite the known, desirable reactive gas solvation properties of PFD, little research has been done on its interaction with plasmas and plasma-produced RONS. Due to experimental challenges to directly and unambiguously measure liquid species, studies of aqueous plasma-liquid interactions often focus on indirect quantification. The most common procedure is to measure products of reactions between plasma-produced species and a dissolved precursor, rather than directly measuring solvated species created in and transported to the liquid phase from the plasma. These reactive targets may be relatively selective (e.g. Griess reagent for nitrite detection [18]) or relatively non-selective (e.g. indigo carmine, often used as a generic indicator of the presence of oxidizing species [19]). In non-aqueous environments such as PFD, however, even these experimental capabilities are limited because hydrophobic PFD will not dissolve the same precursors as water. Additionally, studies that depend on aqueous ions, such as the Griess reagent detection of nitrite, are not possible since species are solvated in PFD in an uncharged state. Thus,

our study of plasma-liquid interactions involving PFD relies mainly on gas phase observations. These observations are used to indirectly infer liquid phase dynamics and species.

In this paper, we study plasma treatment of PFD, both as a liquid-phase target by itself and as a coating on a porous membrane. It will be shown that, as expected, PFD dissolves relatively high concentrations of plasma-produced O_3 and NO_x. The primary dissolved NO_x species will be shown to be NO_2. The relationship between gas-phase NO_2 and N_2O is be explored. We demonstrate the existence of a gas phase NO_2 "burst" as PFD evaporates. Additionally, it will be shown that PFD does not appear to enhance transmission of NO_x through a porous membrane. These observations help provide insight into possible mechanisms by which use of PFD enhances plasma-based treatment of onychomycosis. Based on these insights, it will be suggested that PFD enhances through-nail plasma treatment of onychomycosis by holding RONS, especially NO_2, in contact with the nail at relatively high concentrations and then releasing them into the gas phase when the PFD evaporates.

2 Experimental Setup

Two experimental devices were used in the study of PFD interacting with species created in air plasma. The first plasma source used was a He jet contained inside a chamber purged with dry air. This device was previously described in greater detail [20]. In addition, we utilized plasma-based O_3 generator. Ozone, generated in a stream of pure O_2, was flowed through the jet configuration (with no plasma) at 200sccm and was incident on a cuvette containing approximately 2.9mL of either PFD or H_2O. Dry air was provided to the chamber through the environment inlet at a rate of 1500sccm. Gas-phase O_3 was measured by attaching the chamber exhaust to a gas cell in a Bruker Vertex 70 Fourier Transform Infrared Spectrometer (FTIR). After treatment and

mixing, dissolved O_3 was measured in an Agilent Cary 60 UV-Vis Spectrometer by means of UV absorption at 254nm. The system is diagrammed in Fig. 1.

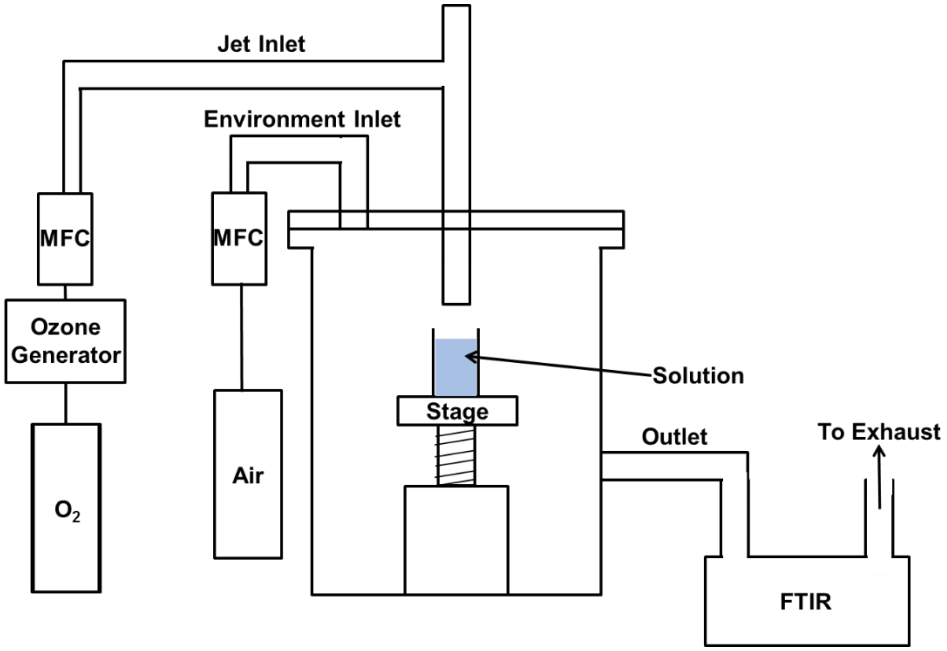

Figure 1. The jet setup for O_3 solvation in water and PFD is shown. A plasma-based O_3 generator provides O_3 to a jet configuration in a chamber containing dry air at atmospheric pressure. The O_3 is incident on a cuvette of PFD or H_2O. Following treatment, O_3 concentration in solution is measured by UV-vis spectrometry. Gas-phase O_3 concentration is measured in the exhaust by FTIR.

The plasma device used for most of the work reported in this paper was a surface microdischarge (SMD). This device was similar to those described previously [15], [21], but smaller in size. In brief, a powered Cu electrode is separated from a grounded steel mesh by a quartz plate. The Cu electrode is 2cm in diameter, and the wire mesh is 3cm in diameter. The discharge is powered at $12kV_{pp}$ with a frequency of 10kHz. A localized plasma is ignited in air immediately adjacent to the grounded mesh, and neutral reactive species diffuse out of the plasma into the surrounding region. The high local electric fields allow for operation in static air, producing relatively large quantities of RONS. Additionally, the localized nature of the plasma and presence of the protective grounded mesh make this source attractive for potential medical applications [15].

The SMD is placed on top of a 'double-decker' two cell chamber, arranged in a Franz cell configuration, as shown in Fig. 2. Each cylindrical cell is approximately 1.4cm tall and 3.9cm in diameter. The cells are connected by a small hole 1cm in diameter, over which can be sealed either a solid barrier (such as a glass slide) or a porous membrane (such as filter paper). The barrier or membrane is sandwiched between two Viton gaskets, with vacuum grease applied to the top and bottom of each gasket, before being clamped down over the hole. The gaskets have a 1cm diameter central hole, exposing the barrier or membrane to the plasma effluent. The barrier or membrane can also be coated with a film of H_2O or PFD. Both the top and bottom cell contain ZnSe windows, each 12.5mm in diameter and 2mm in thickness. These windows are transmissive in the infrared and allow for the gas-phase species to be measured by FTIR absorption spectroscopy. The setup is placed within the light path of the FTIR instrument on a translatable vertical stage that can allow for either the top or the bottom cell to be positioned for FTIR measurement. Before each experiment, the background absorption spectrum is collected. After each experiment, the FTIR spectra are corrected for baseline variations before being fit to molecular spectra calculated from the HITRAN database, as outlined elsewhere [22]. Spectra were taken every minute, with each minute's spectrum consisting of averaged data from 16 consecutive scans; the time required to take the 16 scans was approximately 7-8 seconds. The resolution was $2cm^{-1}$. Individual molecular spectra are fit to non-overlapping regions of the main species quantified in this paper (N_2O, NO_2, and O_3), allowing their concentrations to be determined individually when mixed together. Most of the error results from baseline subtraction, curve-fitting, and run-to-run variation; in the absence of overlapping spectra caused by PFD products, when only small concentrations of the main species are present, the limit of detection is on the order of a few ppm.

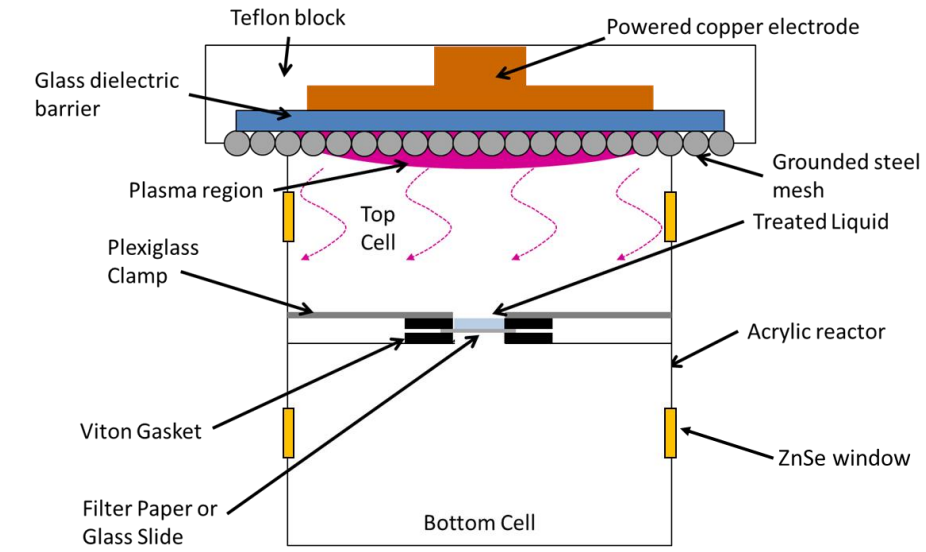

Fig. 2. The SMD system is shown. The SMD is placed on top of a Franz cell-style chamber. The top and bottom cells are connected by a 1cm-diameter hole, over which can be clamped a solid barrier (glass slide) or porous membrane (filter paper). The barrier or membrane can be left dry, or it can be coated with a thin film of H_2O or PFD. Both the top cell and the bottom cell are equipped with ZnSe windows to allow for measurement of gas phase RONS by FTIR. The chamber is placed on a translatable vertical stage that allows the IR beam to pass through either the top ZnSe windows or the bottom ZnSe windows, facilitating FITR measurement of the gas composition in either the top or bottom cell.

3 Results and Discussion

A. Ozone Generation and Solvation

As mentioned in Sec. 1, most liquid-phase diagnostic techniques for plasma-liquid interactions are incompatible with PFD. However, dissolved species with significantly large absorption cross-sections in the UV or visible region can be measured directly via UV-vis absorption spectrometry. Among the RONS produced by atmospheric pressure plasmas, most (including NO_2 and N_2O) have cross sections small enough that they are difficult to measure with our UV-vis spectrometer, given the expected concentrations. Attempts to use UV-vis to measure SMD-generated NO_2 and N_2O dissolved in PFD were unsuccessful. This was not surprising since their absorption cross-sections in this region are on the order of $10^{-19}cm^2$ [23], [24]. However, O_3 has a significantly

larger cross section, reaching a peak value of $1.2x10^{-17}cm^2$ at 254nm and allowing for measurement by UV-vis absorption [25].

To demonstrate the principle of direct measurement of enhanced RONS solvation by PFD, a known controlled system was used. As described in Sec. 2, a commercial O_3 generator was used to provide O_3 through a jet impinging on a cuvette of liquid in an otherwise dry air environment. The O_3 concentration measured by FTIR was calculated to be ~2800ppm. In separate experiments, PFD and H_2O were each treated for 5min. Afterwards, the liquid was capped, wrapped in Parafilm (though the seal was not completely airtight), and vortexed to ensure good mixing throughout the solution volume. This, along with transfer to the UV-vis spectrometer, occurred over the course of ~2 minutes, after which time absorption measurement commenced. As shown in Eq. 1, absorption was converted into concentration by means of the Lambert-Beer Law, where c is concentration, a is absorbance, b is the path length (1cm for the cuvette used in this paper), and ε is the molar extinction coefficient for O_3 (3300L/mol-cm at 254nm [26]). Results are shown in Fig. 3.

$$c = \frac{a}{\varepsilon b} \quad (1)$$

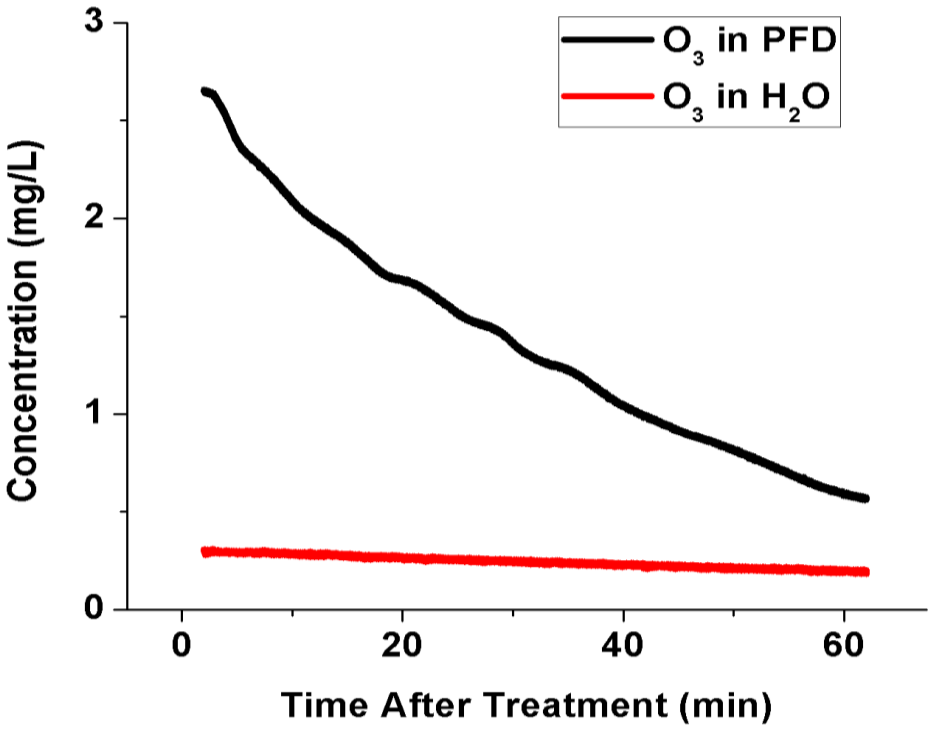

Fig. 3. Dissolved O_3 is measured by UV absorption at 254nm after treatment of PFD and water. The initial concentrations show a dissolved O_3 concentration that is approximately one order of magnitude higher in PFD than in H_2O. This illustrates the enhanced solubility of reactive species in PFD, relative to water. These results are consistent with the work of Li et al. [22]. These authors reported a factor of 15 between concentration of O_3 dissolved in PFD and O_3 dissolved in H_2O.

As shown in Fig. 3, PFD displays an initial post-treatment O_3 concentration an order of magnitude higher than that seen in H_2O. The decay in O_3 liquid-phase PFD concentration over time is largely attributed to a relatively poor seal on the cuvette cap. The order-of-magnitude difference seen in our results is in agreement with Refs. [27]–[29]. These authors reported factors of 10-15 between dissolved O_3 in PFD and dissolved O_3 in H_2O. It should be noted that the earlier works generally relied on indirect measurements such as quantification by means of indigo carmine dye. The results in Fig. 3 demonstrate a similar contrast in water and PFD solubility of O_3 using UV absorption measurements. However, although this experiment demonstrates the proof-of-concept of enhancing RONS solvation with PFD, it is suspected that other species such

as NO_x are important in many applications of plasma to biological targets. Therefore, a study of the more general plasma source capable of producing NO_x, such as an SMD, was undertaken.

B. SMD Generation of NO_x and Effect of NO_2 on N_2O

As mentioned in Sec. 1, quantification of plasma-liquid interactions by solution indicator reactions is difficult in non-aqueous systems. Furthermore, direct UV-vis measurement of dissolved NOx is limited by absorption cross-sections significantly lower than that of O_3. Thus, we decided to characterize plasma-PFD interactions by studying changes in the gas phase adjacent to the liquid. For this reason, the SMD source was attached to the Franz cell as described in Sec. 2, in order to allow for FTIR measurements of gas-phase species.

The simplest experiment, which allows for a "base condition" (12kV, 10kHz, no liquid) against which other experiments can be compared, is to place a dry glass slide between the top and bottom cells of the chamber, sealing the top from the bottom and measuring the gas-phase species generated by the SMD in the absence of any liquid. The results are shown in Figs. 4 and 5.

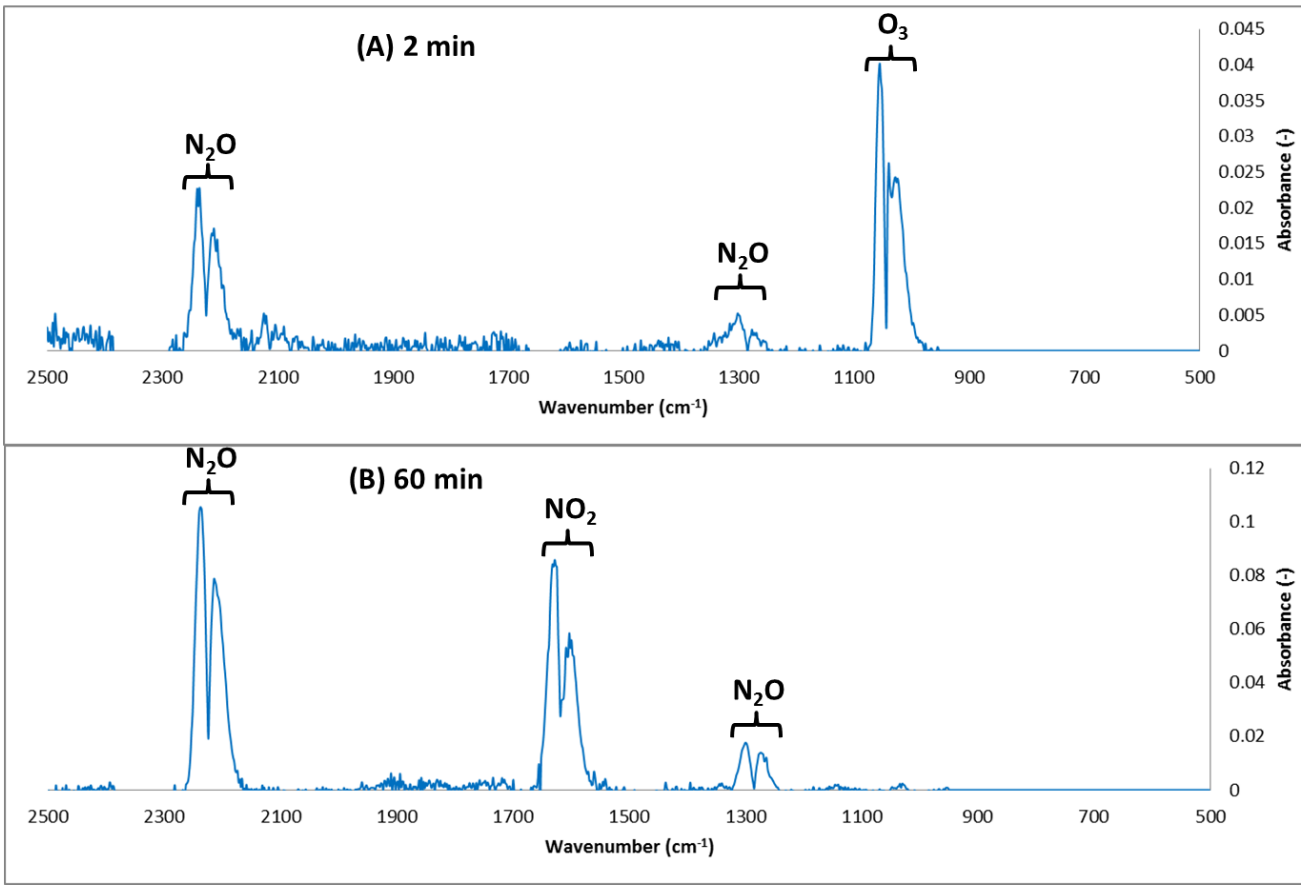

Fig.4. (A) Typical FTIR spectrum of the air SMD output in the top cell after 2min operation using 12kV_{pp}, 10kHz operation. An impermeable, dry glass slide separated the top and bottom cell, resulting in no diffusion of species to the bottom cell. At this relatively early time, the principal long-lived RONS are seen to be O_3 and N_2O. (B) The same experiment is shown after 60min of SMD operation. N_2O remains, but all O_3 has been destroyed, and NO_2 is present instead.

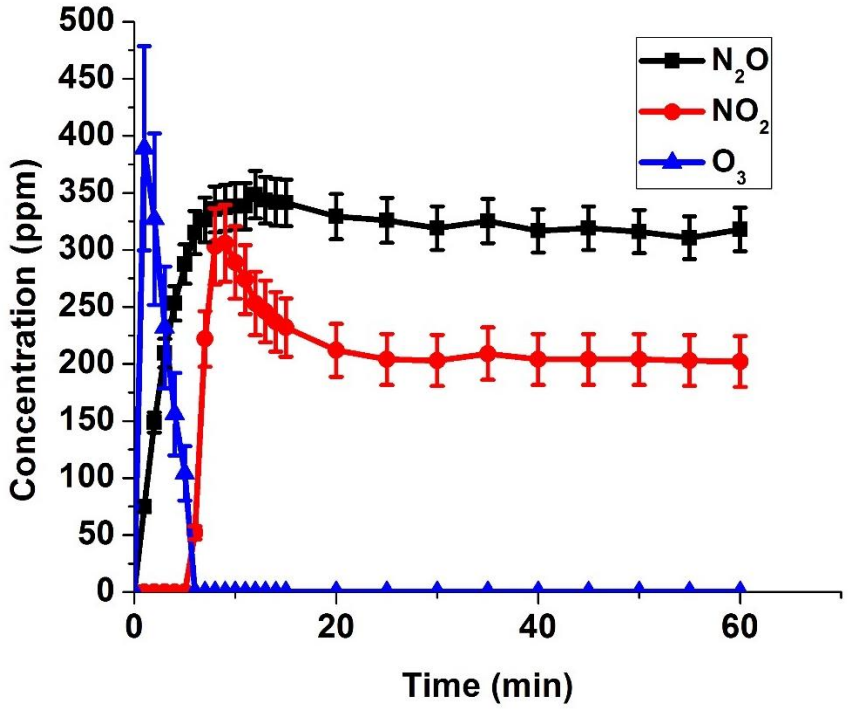

Fig. 5. Gas-phase concentrations from the experiment in Fig. 4 are plotted as a function of time. Within the first few minutes of operation, the SMD exhibits the well-known transition from "O_3 mode" to "NOx mode", as described in, e.g. [22]. N_2O is created from the time of ignition but NO_2 does not appear in measurable quantities until O_3 has been consumed and the mode transition has occurred.

The main species observed are N_2O, NO_2, and O_3. As expected, the plasma demonstrates the well-known transition between the so-called "Ozone Mode" and "NOx Mode" after a few minutes [22]. Over the course of 1hr, most operation takes place in NOx mode. It should be noted that "NOx Mode" is not an absolute nomenclature, since N_2O exists from plasma ignition, along with O_3. The onset of what is termed NOx mode is marked by the appearance of NO_2, which does not exist in measurable amounts until all O_3 has been depleted.

Operation of the SMD in the "base condition" also demonstrated a relationship between NO_2 and N_2O. When voltage and frequency remained constant, quantities such as the steady-state concentration of N_2O were reproducible. However, even when voltage and frequency were constant, one transient effect varied: the appearance time of NO_2. This is not necessarily surprising, as plasmas are strongly nonlinear systems, and imperceptible changes in inputs can

often produce perceptible changes in outputs. However, this allowed for an observation that the existence of NO_2 appears to be correlated with a reduction in the production of N_2O. Though N_2O values reach the same steady state regardless of NO_2 appearance time, they can temporarily reach higher levels if NO_2 does not appear sufficiently early. It should also be noted that the O_3 depletion time also varied with experiment and always corresponded exactly to the appearance time of NO_2. Unlike with O_3, the appearance of NO_2 does not cause an elimination of N_2O; however, it appears to reduce the total source of N_2O. If NO_2 appears within the first few minutes of operation, it is followed by a quick elimination of the rise in N_2O, the concentration of which quickly reaches a steady state. If NO_2 appears later (and N_2O has temporarily reached higher values), the appearance of NO_2 is followed by a decrease in N_2O until steady state is achieved. This effect is illustrated in Fig. 6.

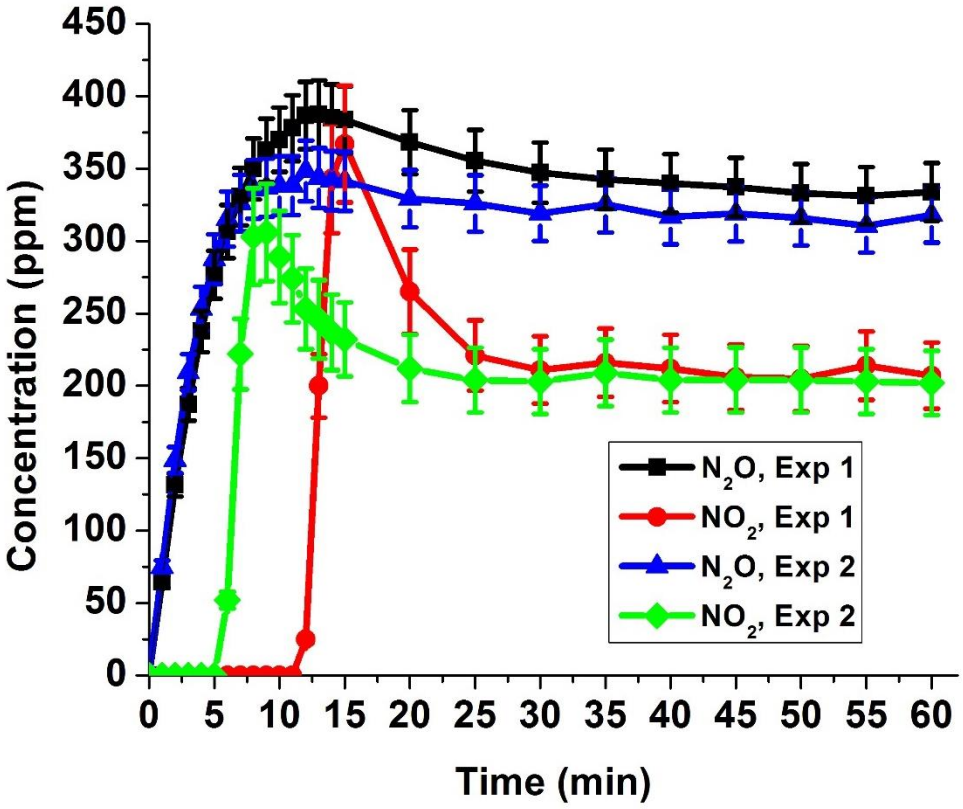

Fig. 6. Two experiments at the base condition ($12kV_{pp}$, 10kHz) are shown. In these experiments, NO_2 first appears at different times (6min vs. 13min). When NO_2 appears, the source of N_2O is reduced. Before NO_2 appears, both experiments show the same rate of rise for N_2O. At 6min, NO_2 appears in Experiment 2, the N_2O rate of rise quickly drops to 0, and steady state is quickly reached. Since NO_2 does not appear until 13min in Experiment 1, N_2O continues to rise to higher concentrations; after NO_2 appears at 13min, N=O decreases until it reaches the same steady-state concentration seen in Experiment 2.

To the authors' knowledge, this is the first time this relationship between NO_2 and N_2O has been demonstrated in a plasma source. While the chemical pathway is not known with certainty, we suspect it may be due to the scavenging of ground-state and excited O atoms by NO_2, which is also one of the mechanisms by which NO_2 impedes O_3 production [21], [30]:

$$NO_2 + O \rightarrow NO + O_2 \quad \text{(R1)}$$

$$NO_2 + O^1{}_D \rightarrow NO + O_2 \quad \text{(R2)}$$

The rate constant of R1 at room temperature is approximately $10^{-11}cm^3/sec$, and the rate constant of R2 at room temperature is approximately $3x10^{-10}cm^3/sec$ [31], [32]. While N_2O is thought to be created largely by the reaction of excited N_2 with ground-state O_2 [33], both ground-state O and excited atomic oxygen ($O^1{}_D$) can react with N_2 and a third body to form N_2O:

$$N_2 + O + M \rightarrow N_2O \quad \text{(R3)}$$

$$N_2 + O^1{}_D + M \rightarrow N_2O \quad \text{(R4)}$$

The rate constants at room temperature are on the order of $10^{-38}cm^6/sec$ and $10^{-36}cm^6/sec$ for R3 and R4, respectively [34], [35]. Thus, R3 and R4 are not insignificant but are small compared with R1 and R2, leading to a reduction in N_2O production once NO_2 appears. However, since R3 and R4 are not the main pathways of N_2O formation, the concentration of N_2O does not follow that of O_3, which decays to 0 due to reaction with NO_2 even before measurable amounts of NO_2 are present.

C. Treatment of 50uL PFD

The next step was to measure gas phase species evolution in the presence of a small quantity of PFD. For this experiment, 50uL PFD was placed on top of the glass slide before plasma treatment. The gasket and clamp above the glass slide created a cup-like shape that confined the PFD. 50uL was chosen because it was observed that evaporation would not significantly reduce its volume during 1hr of plasma treatment. The corresponding FTIR absorption spectrum of the gas phase in the top cell is shown in Fig. 7.

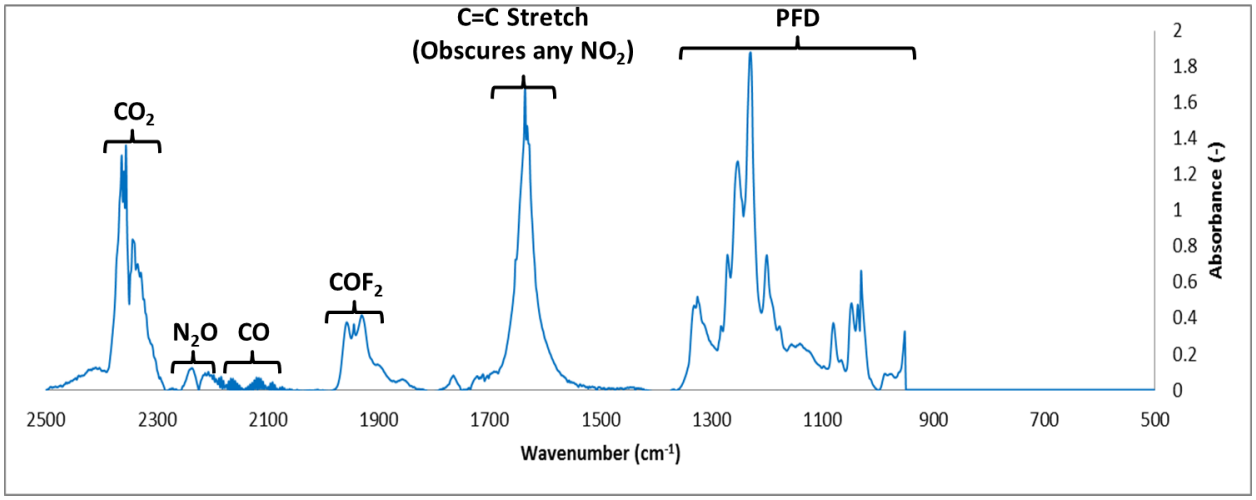

Fig. 7. When 50uL of PFD is present in the top cell, several new features are observed in the gas phase by FTIR. Notably, gas-phase PFD completely obscures O_3, while a C=C stretch obscures NO_2. COF_2, CO, and CO_2 are also present, apparently as reaction products of gas-phase PFD reacting with air in the plasma. N_2O measurement is not obscured and can still be quantified.

As shown in Fig. 7, PFD introduces several new features to the FTIR spectrum. Between approximately 950 and 1300cm^{-1}, a spectrum corresponding to gas-phase PFD can be observed. PFD at room temperature has a vapor pressure of approximately 6.75 Torr [36]. Although this is a factor of 4 smaller than that of H_2O, gas-phase PFD will still be present in significant quantities when liquid phase PFD is present. At the other end of the spectrum are some products apparently generated by gas-phase PFD entering the plasma, dissociating, and forming reaction products with

air. Near 2350cm^{-1} is CO_2, while CO is seen near 2150cm^{-1} and COF_2 is seen near 1950cm^{-1}. Finally, a large peak is seen at approximately 1645cm^{-1}. While NO_2 and H_2O both have peaks within this regime, neither correspond to the shape of the observed peak, and it only appears when PFD is present. The shape and location of this peak are consistent with a double-bonded carbon (C=C) stretch [37], which is most likely the cause of this feature. Unfortunately, the PFD spectrum and the C=C stretch virtually completely obscure the detection of O_3 and NO_2, respectively. However, N_2O measurement is unperturbed. Figure 8 illustrates the time evolution of N_2O under base conditions ("Dry") and in the presence of 50 μL PFD.

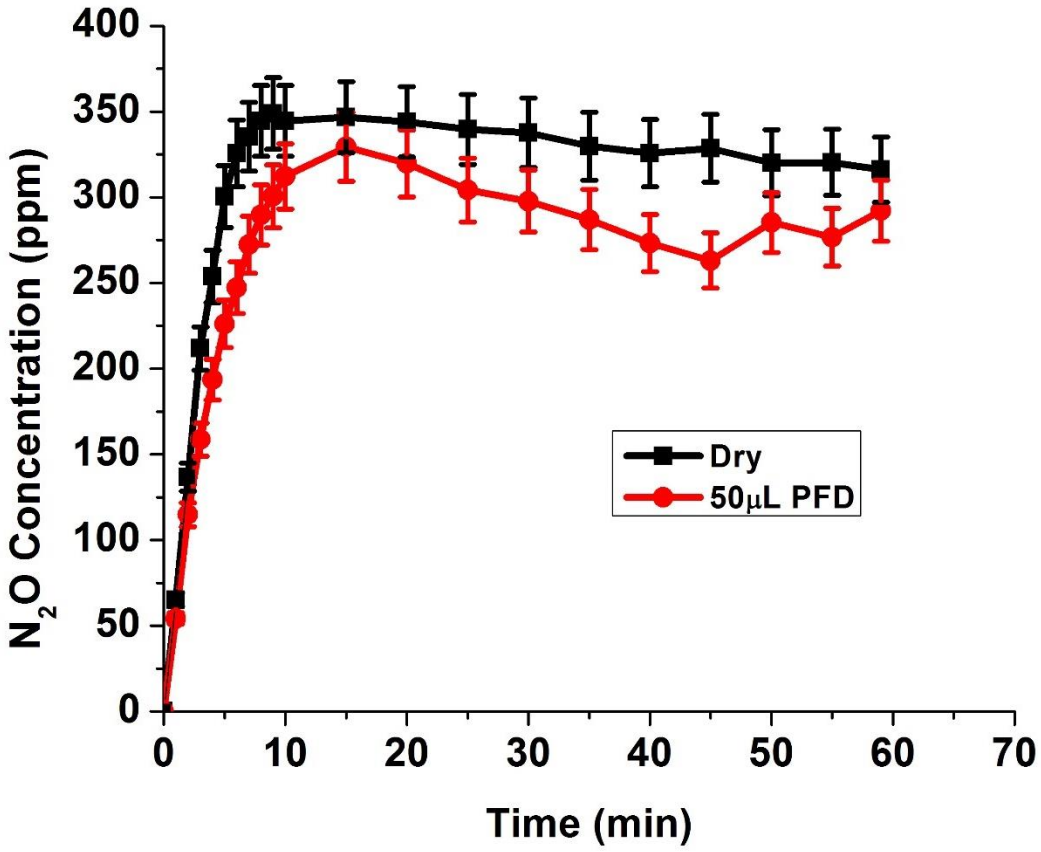

Fig. 8. N_2O is measured in the gas phase with and without 50uL of PFD present. The final steady-state values of N_2O show no significant difference. This is expected due to the calculated Henry's Law equilibrium liquid-phase concentration of 405μM, which is only expected to change the gas-phase concentration by 28ppm. However, the rise of N_2O is slower in the presence of PFD than in the dry experiment.

In Fig. 8, it is shown that N_2O in the presence of PFD rises more solwly initially, before reaching a similar steady-state value as seen for N_2O in the absence of PFD. This is in agreement with Henry's Law and mass balance considerations. Solubility constants for non-O_2 gases in PFD are difficult to find in published literature. However, Moshnyaga et al. [38] reported an equivalent Henry's Law coefficient, k_H, of 1.3mol/L-atm at room temperature. The equilibrium concentration of dissolved N_2O in PFD can then be calculated from the definition of Henry's Law coefficient,

$$c_{liq}\left[\frac{mol}{L}\right] = k_H \frac{mol}{L \cdot atm}\ c_{gas}[atm] \tag{2}$$

For a gas-phase concentration of 310ppm, this corresponds to approximately 405μM in the liquid phase. To estimate the expected effect on the gas phase, a mass balance equation is carried out to determine the amount by which the gas phase concentration would increase if the dissolved N_2O were released back into the gas phase:

$$\Delta c_{gas} = \frac{c_{liq} V_{liq}}{V_{gas}} \tag{3}$$

For a liquid-phase concentration of 405μM, this corresponds to a gas-phase concentration difference of approximately 28ppm. This difference is easily within the error bars seen in Fig. 8, so it is not unexpected that the presence of liquid PFD under these conditions would not appreciably affect the gas phase concentration of N_2O.

Although the measurement and analysis appear consistent, the observation raises the question: What can be learned about plasma-PFD interactions if the main species that is directly quantifiable does not exhibit a significant difference in the gas phase? The answer lies in considering the transient evaporation of PFD and in recognizing that other species (notably NO_2) can still be observed in the gas phase, albeit indirectly.

D. Evaporation of PFD During Treatment: Treatment of 5uL PFD

As mentioned in Sec. 3C, PFD evaporates during plasma treatment due to its significant vapor pressure under experimental conditions. In fact, if the original amount of PFD were small enough, the entire liquid phase would evaporate during treatment. We chose to explore this transition to further shed light on the gas and liquid dynamics of the system.

To ensure that all PFD would evaporate, the relatively small initial volume of 5μL was chosen. A background spectrum was taken before application of PFD in order to ensure that the PFD spectrum was truly a measure of the amount of PFD present in the gas phase. Results are shown in Figs. 9 and 10.

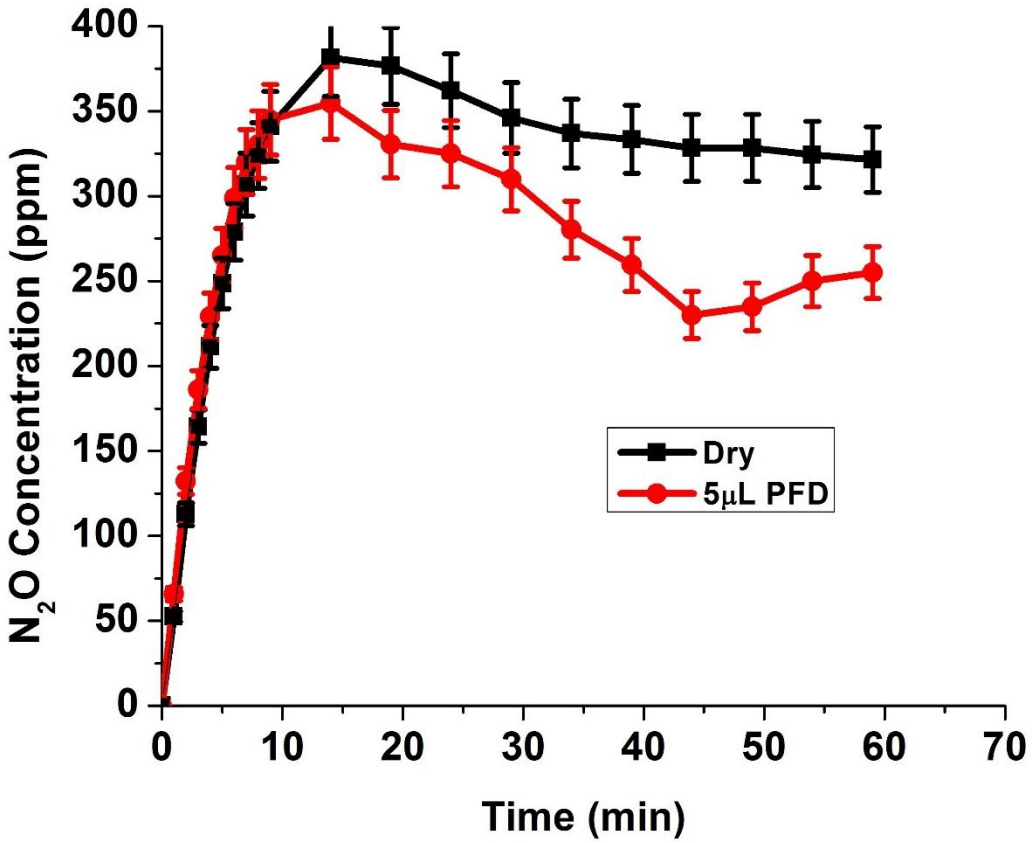

Fig. 9. When 5μL of PFD are treated, gas-phase N_2O at first remains within error of N_2O without PFD present. At 30min, however, the concentrations begin to diverge. The cause is the evaporation of PFD and sudden release of NO_2 (shown in Fig. 10). This release of NO_2 into the gas phase lowers the amount of N_2O but it does not constitute a long-term source of NO_2. Thus, the N_2O starts to rise back towards its steady state value after ~40min.

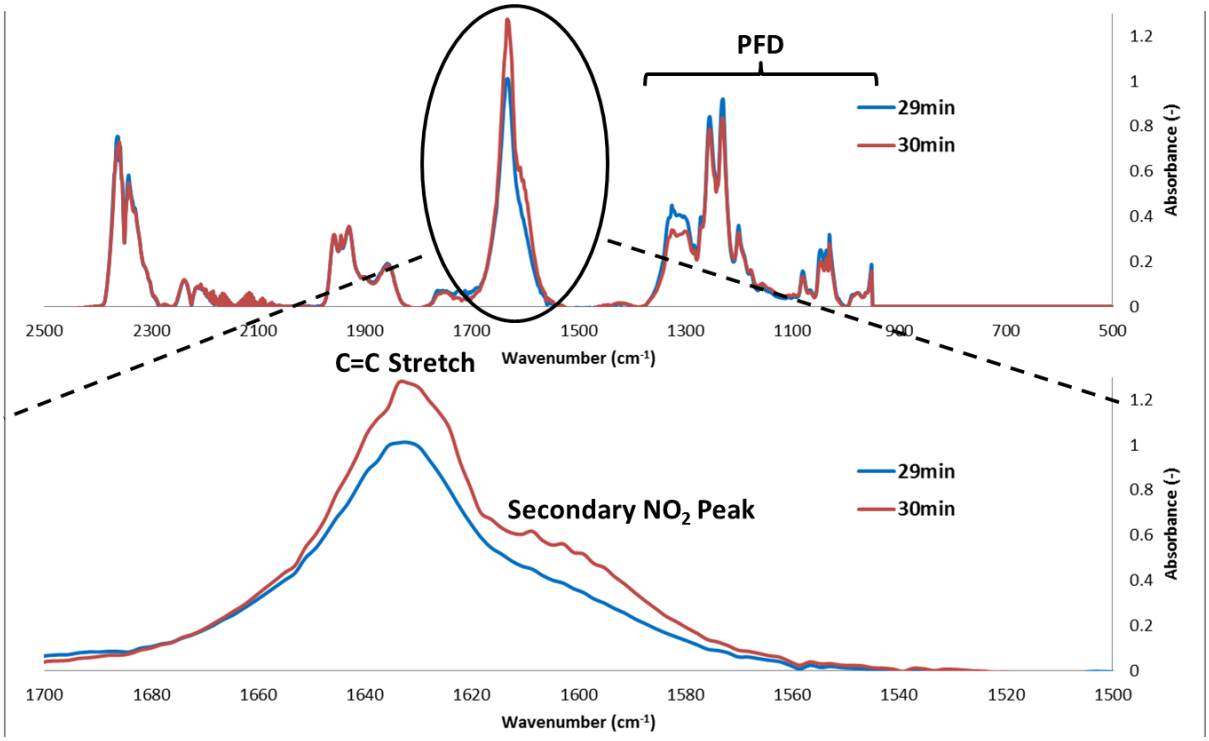

Fig. 10. (Top) FTIR spectra of the 5µL experiment are shown at 29 and 30min. At 30min, the PFD signal begins to decrease, indicating that the source of gas-phase PFD has disappeared and that the liquid phase has completely evaporated. (Bottom) The complete evaporation of the liquid phase at 30min also coincides with a sudden release of NO_2 into the gas phase. While the C=C stretch still eliminates the ability to quantify NO_2 and the peak of the C=C stretch overlaps with the location of the dominant NO_2 peak, a feature corresponding to the location of the second NO_2 peak suddenly appears at 30min, indicating that NO_2 previously dissolved in PFD has now been released into the gas phase.

As seen in Fig. 9, the N_2O concentration in the presence of PFD is initially within measurement error of the concentration without PFD present. However, after 30min of treatment, the N_2O concentration suddenly drops. This occurs in tandem with the complete evaporation of the PFD. As shown in Fig. 10, the PFD spectrum begins to decrease in magnitude at 30min, indicating that the liquid-phase source of gas-phase PFD is gone. It should be noted that the evaporation of PFD is significantly faster with plasma present than without plasma present, due to both plasma heating and plasma-induced reactions that consume gas-phase PFD. At the same time, a feature appears on the right side of the C=C stretch, corresponding to the location of the lesser NO_2 peak. Since the larger NO_2 peak is overlapped by the peak of the C=C stretch, it is difficult to distinguish that

peak independently; however, the secondary NO_2 peak at approximately 1600cm^{-1} can be seen. Attempting to fit a combination the 29min spectrum and an NO_2 spectrum to the 30min data does yield a good reproduction of the 30min data, but the error bar on the NO_2 fit is on the order of 100ppm. Despite the difficulty with precision, the appearance of the feature at 1600cm^{-1} qualitatively indicates a substantial rise in the gas-phase NO_2. We assert that this corresponds most likely to NO_2 which has been released by the evaporation of the PFD.

The evaporation of PFD is followed by a corresponding significant reduction in N_2O. The magnitude of this reduction is on the order of 100ppm under the conditions we studied. This effect causes a significant departure from the N_2O concentration as compared to the dry experiment. Additionally, the N_2O production increases again between 45 and 60min. This is suggests a temporary, rather than permanent, reduction in the source of N_2O.

Taken together, these results are consistent with the relationship between NO_2 and N_2O described in Sec. 3B, and they imply a sudden release of NO_2 from the evaporating liquid phase. The suggested series of events is as follows. Evaporation of PFD is accelerated by plasma heating and by reactions that consume gas-phase PFD. As PFD evaporates, it continues to hold NO_2 in the liquid phase with ever-increasing concentrations. The fast PFD evaporation does not give time for NO_2 to slowly leave the liquid phase and re-establish Henry's Law equilibrium. Thus, the liquid-phase concentration of NO_2 increases with this loss of liquid PFD. At 30min, the PFD evaporates completely, releasing a burst of NO_2 into the gas phase and causing the appearance of the NO_2 peak shown in Fig. 10. The sudden increase in the gas-phase NO_2 concentration causes a reduction in the production of N_2O. Accordingly, the measured concentration of N_2O in the gas phase decreases. However, evaporation of the PFD is only a transient source of NO_2, and the

temporary increase in gas-phase NO_2 cannot be sustained. Because of this, the N_2O concentration begins to rise again in the last 15min of treatment.

This interpretation suggests that the PFD dissolves a relatively large amount of NO_2, probably considerably larger than the amount of N_2O that it dissolves. Evidence for this assertion will be shown in the following section.

E. Evaporation of Plasma-Activated PFD

Since NO_2 is difficult to measure directly in the gas phase during treatment of PFD and is also not easily measurable by UV absorption or indicator techniques in the liquid phase, a different method was chosen to obtain information about NO_2 solvation in PFD. Many plasma biomedicine studies make use of investigations involving plasma-activated water (PAW), in which water is plasma-treated before being applied to a desired surface. In this section, we describe an investigation of plasma-activated PFD. This set of experiments of NO_2 leaving previously-treated PFD provides additional evidence for our interpretation of events.

In this set of experiments, the glass slide between the top and bottom cell was removed, and a small cuvette approximately 1cm on each side was placed over the hole between the cells. 50μL of PFD were placed in the cuvette, and the PFD was treated by the SMD plasma for 1hr. Following this, the SMD was removed, the cuvette was removed, and the chamber was purged with compressed air for approximately 10min. During purging, the plasma-activated PFD (PA-PFD) was mixed with a pipette. While not directly mixed, the cuvette was capped and wrapped in Parafilm. After purging, 10μL of PA-PFD was pipetted into the bottom cell of the chamber. The SMD was then replaced but not powered, and the gas phase IR spectrum was monitored in the bottom cell as the PA-PFD began to evaporate and release dissolved gases back into the gas phase. A sample FTIR spectrum from a typical experiment is shown in Fig. 11.

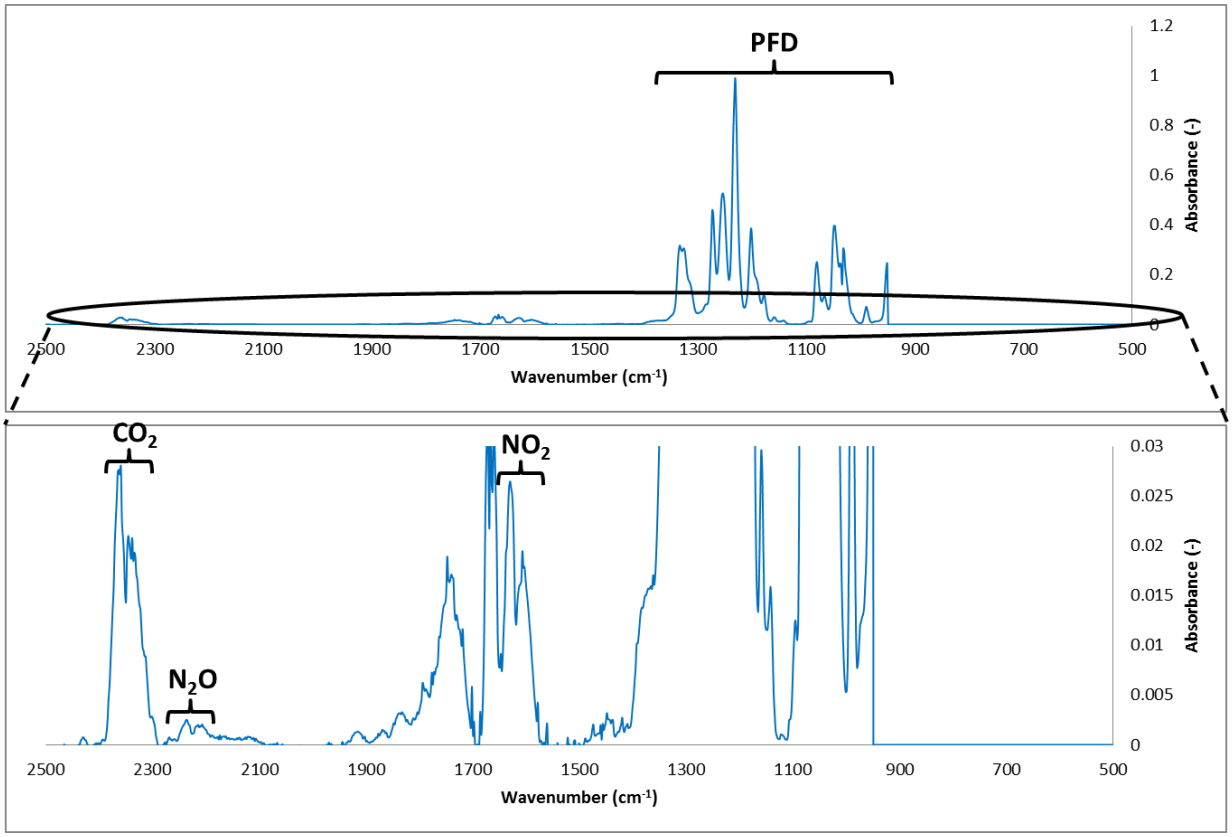

Fig.11. A spectrum taken during evaporation of PA-PFD is shown. Unsurprisingly, the dominant feature is PFD itself. However, a significant amount of NO_2 (approximately 120ppm) is observed to leave the liquid-phase PFD and enter the gas phase.

The amount of NO_2 entering the gas phase from the liquid phase is large enough to be measured and plotted as a function of time. Results are shown in Fig. 12, with the PA-PFD inserted into the chamber between 0min and 1min.

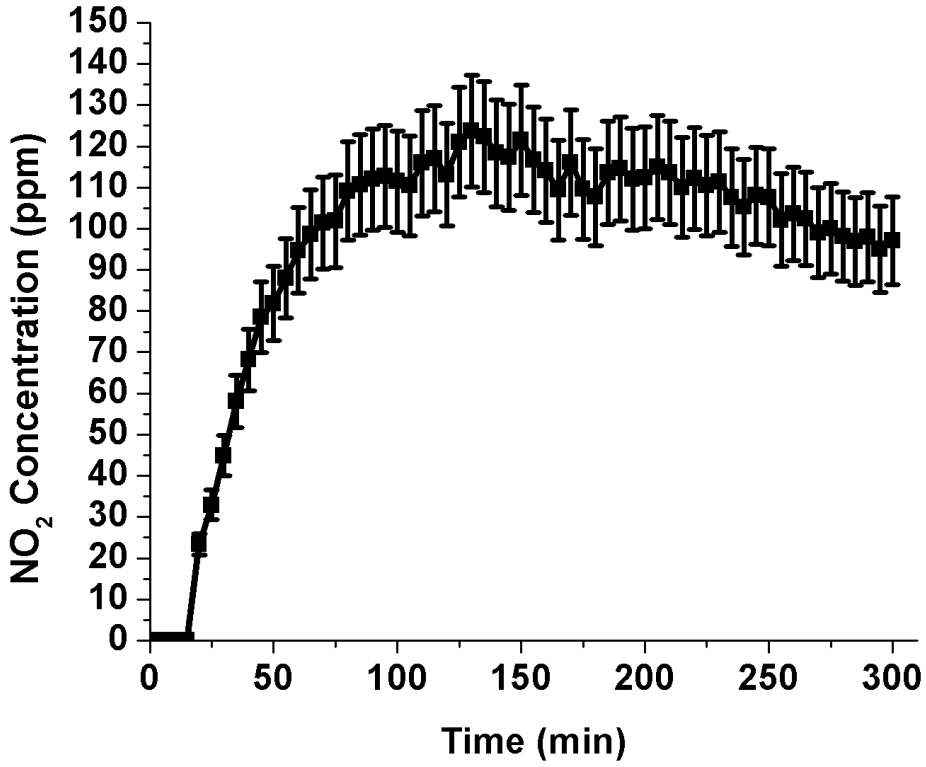

Fig. 12. After treating 50uL of PFD for 60min, the PFD is removed and 10uL is re-inserted. The gas-phase NO_2 signal is monitored while the 10uL of PA-PFD evaporates. For the first 15min, NO_2 remains completely in the liquid phase. Afterwards, NO_2 begins to enter the gas phase, reaching a peak concentration of approximately 120ppm.

Even after remaining in the cuvette for 10min prior to insertion into the bottom cell, it takes the PA-PFD more than 15min to begin emitting measurable quantities of NO_2. This is another indicator of the strong affinity NO_2 has for PFD. As liquid PFD evaporates, the peak NO_2 concentration reaches approximately 120ppm. The subsequent, relatively slow decrease of NO_2 is likely due to leakage from the chamber.

The fact that ~120ppm of NO_2 is released into the gas phase from just a 10uL sample of PA-PFD demonstrates the power of PFD to dissolve and retain NO_2. Since there is no other source of NO_2, all of the measured NO_2 must have come from the PFD. If the same mass balance calculation from Sec. 3C is reversed, it is found that, given the large size of the chamber volume relative to the 10uL PFD volume, putting 120ppm of NO_2 into 10uL of PFD would cause the liquid-phase concentration of NO_2 to be ~18mM. Thus, PA-PFD after 1hr of plasma treatment contained at

least 18mM NO_2. This is significantly higher than the N_2O liquid-phase concentration calculated from Henry's Law (405μM). It is also of interest that, while small amounts of N_2O are observed to enter the gas phase, they are relatively small (on the order of 7ppm) in comparison to the measured NO_2 concentrations and often dominated by noise. As a side note, it should be observed that this is not inconsistent with the earlier predictions about dissolved N_2O, as these results suggest that evaporation of a 50uL volume (as opposed to a 10uL volume) would have released approximately 35ppm into the gas phase. Since the chamber size is effectively doubled by removing the glass slide, this would correspond to 70ppm if the PFD were evaporated in the top chamber alone; this figure is on the same order as the 28ppm figure predicted from Henry's Law in Sec. 3C.

We are not aware of any published Henry's Law coefficient values for NO_2 in PFD; these results imply that either its value is unusually large (even compared to the coefficient for N_2O in PFD), or NO_2 is formed through reactions between other RONS species dissolved in PFD, or both. These results also demonstrate the relatively high abundance of NO_2 in the liquid phase and suggest that, for an SMD operating in NOx mode, NO_2 is a leading candidate as for the observed PFD-enhanced plasma treatment of onychomycosis. This is consistent with related studies coupling a mathematical model of reaction and diffusion of NO_2 through porous keratin. (Im et al., submitted, 2018)

E. NOx Transmission Through a Porous Membrane

The results shown so far have demonstrated that, in plasma-PFD interactions, PFD appears to dissolve realtively high concentrations of NO_2 before releasing the NO_2 in a burst as the PFD evaporates. While this process alone is a plausible explanation of how PFD enhances through-nail plasma treatment of onychomycosis, another possible interpretation is that PFD increased

exposure of fungi growing between the nail and the skin to lethal NOx by enhancing transport of NOx through the nail. We show results in this section suggesting that this interpretation is unlikely.

To test whether or not PFD enhances transport (diffusion) through a porous membrane, we conducted a series of experiments using Whatman Grade 1 filter paper as a sample porous material. This material is considerably more porous than keratin and should therefore show PFD-induced enhanced transport if it is present. However, it is not the same composition as keratin, of course, and additional experiments are needed to thoroughly validate the conclusion. It should be noted that, while filter paper is generally a poor substitute for living tissue, a dry nail (unlike living tissue) is not expected to have significant water content from biological sources. Rather, the fibers of a dry nail are coated with a layer of adsorbed water from the air [39]; the filter paper should be similar in this regard.

In this set of experiments, the glass slide was removed and replaced with filter paper, which allowed for transmission of gas-phase species between the top and bottom cells. As with the glass slide, liquid can be inserted on top of the filter paper. Experiments were performed with the filter paper dry, water-coated, and PFD-coated. Due to relative ease of measurement, N_2O concentration was monitored in the bottom cell in order to quantify membrane transmission. Plasma treatment was carried out for 60min, after which the SMD was turned off and species decay was measured for 60min. Results are shown in Fig. 13.

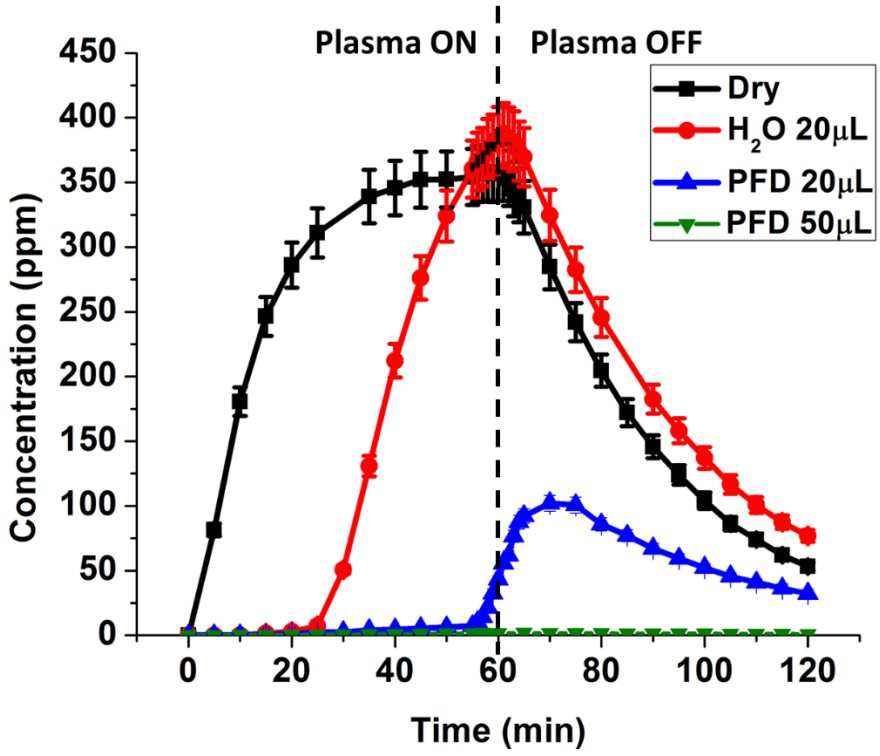

Fig. 13. Experiments are performed to determine if the presence of PFD raises transmission through a porous membrane into the gas phase on the far side. The glass slide is replaced with filter paper, and N_2O concentrations are measured in the bottom cell. N_2O readily penetrates the filter paper when the paper is dry, but it does not penetrate the porous materials in the presence of liquid. Both H_2O and PFD act as barriers until enough evaporates to restore transmissivity to the filter paper. Due to its higher vapor pressure, H_2O evaporates more quickly, and N_2O concentrations reach their dry values correspondingly faster. In the case of 20uL PFD, transmissivity is restored near 60min, so N_2O does not reach the bottom cell until approximately the time that the plasma is turned off. For 50uL PFD under these experiments, PFD remains in sufficient quantities on the filter paper that almost all transmission of N_2O to the lower cell is blocked.

When the filter paper is dry, it is quite transmissive, allowing N_2O concentrations in the bottom cell to rise quickly. However, this is not the case if either H_2O or PFD are present. If 20uL H_2O, 20uL PFD, or 50uL PFD is added on top of the filter paper, transmissivity drops to nearly 0, and very little N_2O initially reaches the bottom cell. Both PFD and water function as barriers to transmission. Though PFD can dissolve considerably more N_2O than water, it does not release the N_2O into the gas phase on the bottom side of the filter paper. Thus, both water and PFD initially function as barriers. During treatment of 20uL H_2O, enough H_2O evaporates that the membrane

becomes transmissive again for approximately the last 20min of treatment. This does not mean all water is completely evaporated; rather, it indicates that the remaining water no longer forms an uninterrupted seal that blocks the transmission of N_2O. Due to the lower vapor pressure of PFD, the same scenario does not begin to occur for 20uL PFD until nearly 60min of treatment time have elapsed. Since the plasma source is turned off at 60min, the bottom cell is not able to reach the same N_2O concentrations as seen in the dry experiment before the source is turned off. For a situation in which sufficient evaporation does not occur, results of a 50uL experiment are also shown. In this case, almost all transmission of N_2O through the filter paper is inhibited. It should also be noted that experiments (not shown) with a 200um-thick slice of bovine hoof showed very little transmission of N_2O to the bottom cell when dry, and that PFD did not increase this transmissivity. Finally, it should be noted that though N_2O is employed in these experiments because it is relatively easy to measure, no other RONS were observed to enter the bottom cell when either the filter paper or nail was not transmissive to N_2O.

The results presented in this section support our conclusion that PFD does not enhance transmission of NOx through a porous membrane. PFD has been shown to be an effective solvent for plasma-generated (and other) gases, it apparently retains dissolved species in the liquid phase and does not re-emission on the unexposed side. We conclude that PFD increases the effectiveness of through-nail plasma treatment by retaining NOx in contact with the nail in relatively high concentrations. NOx species are released in a burst upon complete PFD evaporation, rather than by enhancing transmission of NOx through the porous nail.

4 Conclusions

Plasma-liquid interactions are of great interest for better understanding the mechanisms of plasma-induced medical treatments and improving such treatments. Recently, it was shown that

perfluorodecalin increased the effectiveness through-nail plasma treatment of onychomycosis, but the science behind the mechanism of this enhancement was unclear.

In this paper, the use of PFD as a strong solvent for plasma-liquid interactions was detailed for the first time. While direct measurement of dissolved species in PFD is difficult, a number of direct and indirect techniques yielded information about the underlying mechanisms. It was shown that PFD, as expected, dissolved high amounts of plasma-produced O_3 and NOx. Based on evaporation of plasma-activated PFD, it was shown that, when the plasma source was an SMD operating in NOx mode, the primary dissolved species was NO_2. Despite gas-phase concentrations on the order of 200ppm in a dry environment, 50uL of PFD was estimated to contain over 18mM NO_2.

A relationship was found between NO_2 and N_2O whereby the presence of gas-phase NO_2 reduces the source of N_2O. It is hypothesized that this relationship is related to reactions between NO_2 and O atoms. Based on this relationship and FTIR spectra, it is shown that evaporation of PFD during plasma treatment releases NO_2 in a burst. Additionally, it was shown that PFD does not enhance transmission of gas-phase RONS through a porous membrane and back into the gas phase on the far side. Instead, application of PFD to a porous membrane acted as a barrier to transmission, confining RONS to the liquid phase and to the gas-phase volume on the near side of the membrane.

Accordingly, the results of this paper suggest that PFD does not enhance through-nail plasma treatment of onychomycosis by increasing transmission of RONS through the nail and back into the gas phase on the far (infected) side. Rather, the evidence suggests that the mechanism of enhancement is caused by PFD holding large high concentrations of NO_2 in contact with the infected nail, only releasing the NO_2 back into the gas phase as a burst upon PFD evaporation. It

should also be noted that the effect, if any, upon antifungal treatment of species produced by plasma fragmentation of PFD has not yet been studied.

Additionally, the results of this paper suggest that PFD could be used in other plasma treatments as well, not just treatment of onychomycosis. Any situation where enhanced solvation of RONS is desirable could potentially benefit from the use of PFD. This represents a promising area of future research.

Acknowledgments

This material is based upon work supported by *Department of Energy OFES grant # DE-SC0001934, NSF award # 1415022, and DoE grant # SC0012500*. The authors would also like to thank Annie Preece-Scaringe and Jeremy Lan for help in carrying out experiments.

References

[1] S. M. Thagard, R. M. Sankaran, and M. J. Kushner, "Science Challenges in Low-Temperature Plasma Science and Engineering : Enabling a Future Based on Electricity Through Non-Equilibrium Plasma Chemistry," NSF Workshop, 22-23 Aug. 2016, Arlington, VA, NSF Report, 2017.

[2] D. B. Graves, "Low temperature plasma biomedicine: A tutorial review," *Phys. Plasmas*, vol. 21, no. 8, 2014.

[3] D. B. Graves, "The emerging role of reactive oxygen and nitrogen species in redox biology and some implications for plasma applications to medicine and biology," *J . Phys . D Appl . Phys .*, vol. 45, no. 45, pp. 263001–42, 2012.

[4] R. S. Tipa, B. Boekema, E. Middelkoop, and G. M. W. Kroesen, "Cold plasma for bacterial inactivation," *Proc. 20th Int. Symp. Plasma Chem.*, 2012.

[5] G. Bauer and D. B. Graves, "Mechanisms of Selective Antitumor Action of Cold Atmospheric Plasma-Derived Reactive Oxygen and Nitrogen Species," pp. 1157–1178, 2016.

[6] D. B. Graves, "Mechanisms of Plasma Medicine : Coupling Plasma Physics , Biochemistry , and Biology," vol. 1, no. 4, pp. 281–292, 2017.

[7] D. Yan, J. H. Sherman, and M. Keidar, "Cold atmospheric plasma , a novel promising anti-cancer treatment modality," vol. 8, no. 9, pp. 15977–15995, 2017.

[8] H. Tanaka, M. Mizuno, K. Ishikawa, K. Takeda, H. Hashizume, and K. Nakamura, "Glioblastoma Cell Lines Display Different Sensitivities to Plasma-Activated Medium," vol. 2, no. 2, pp. 99–102, 2018.

[9] X. Liu *et al.*, "A comparative study on the transdermal penetration effect of gaseous and aqueous plasma reactive species," *J. Phys. D. Appl. Phys.*, vol. 51, no. 7, 2018.
[10] P. J. Bruggeman *et al.*, "Plasma–liquid interactions: a review and roadmap," *Plasma Sources Sci. Technol.*, vol. 25, no. 5, p. 053002, 2016.
[11] I. R. Schmolka, "Artificial Blood Emulsifiers," US4395393, 1983.
[12] Q. A. Tawfic and R. Kausalya, "Liquid ventilation," *Oman Med. J.*, vol. 26, no. 1, pp. 4–9, 2011.
[13] S. Moradi, A. Jahanian-Najafabadi, and M. H. Roudkenar, "Artificial blood substitutes: First steps on the long route to clinical utility," *Clin. Med. Insights Blood Disord.*, vol. 9, pp. 33–41, 2016.
[14] D. R. Spahn, "Blood substitutes: Artificial oxygen carriers: Perfluorocarbon emulsions," *Crit. Care*, vol. 3, no. 5, pp. 93–97, 1999.
[15] Z. Xiong, J. Roe, T. C. Grammer, and D. B. Graves, "Plasma Treatment of Onychomycosis," *Plasma Process. Polym.*, vol. 13, no. 6, pp. 588–597, 2016.
[16] J. N. Roe, T. C. Grammer, and M. P. O'Neill, "Onychomycosis Treatment Apparatus and Method," US20160166607A1, 2016.
[17] B. D. Spiess, "Perfluorocarbon emulsions as a promising technology: a review of tissue and vascular gas dynamics," *J. Appl. Physiol.*, vol. 106, no. 4, pp. 1444–1452, 2009.
[18] D. Tsikas, "Methods of quantitative analysis of the nitric oxide metabolites nitrite and nitrate in human biological fluids," *Free Radic. Res.*, vol. 39, no. 8, pp. 797–815, 2005.
[19] E. H. Harris, M. I. Lokanathan, and B. D. Hench, "Device Use Indicator," 6314907B1, 2001.
[20] D. T. Elg, I. Yang, and D. B. Graves, "Production of TEMPO by O atoms in atmospheric pressure non-thermal plasma–liquid interactions," *J. Phys. D. Appl. Phys.*, vol. 50, no. 47, p. 475201, 2017.
[21] M. J. Pavlovich, H.-W. Chang, Y. Sakiyama, D. S. Clark, and D. B. Graves, "Ozone correlates with antibacterial effects from indirect air dielectric barrier discharge treatment of water," *J. Phys. D. Appl. Phys.*, vol. 46, no. 14, p. 145202, 2013.
[22] M. J. Pavlovich, D. S. Clark, and D. B. Graves, "Quantification of air plasma chemistry for surface disinfection," *Plasma Sources Sci. Technol.*, vol. 23, no. 6, p. 065036, 2014.
[23] N. Rontu Carlon, D. K. Papanastasiou, E. L. Fleming, C. H. Jackman, P. A. Newman, and J. B. Burkholder, "UV absorption cross sections of nitrous oxide (N_2O) and carbon tetrachloride (CCl4) between 210 and 350 K and the atmospheric implications," *Atmos. Chem. Phys.*, vol. 10, no. 13, pp. 6137–6149, 2010.
[24] M. H. Harwood and R. L. Jones, "Temperature dependent ultraviolet-visible absorption cross sections of NO_2 and N_2O_4 : Low-temperature measurements of the equilibrium constant for $2NO_2$ <--> N_2O_4," *J. Geophys. Res.*, vol. 99, no. D11, pp. 22,955-22,964, 1994.
[25] L. T. Molina and M. J. Molina, "Absolute absorption cross sections of ozone in the 185- to 350-nm wavelength range," *J. Geophys. Res.*, vol. 91, no. D13, pp. 14501–14508, 1986.
[26] C. I. Koh, S. J. Lee, and J. W. Kang, "New UV-flux measurement method using ozone photolysis rate," *Ozone-Science Eng.*, vol. 23, no. 3, pp. 245–253, 2001.
[27] S. Li, Y. Zhu, and X. Li, "Degradation p-Chloronitrobenzene in Ozone-loaded System with Perfluorodecalin Solvent," pp. 297–302, 2011.
[28] D. Bhattacharyya, T. F. Van Dierdonck, S. D. West, and A. R. Freshour, "Two-phase ozonation of chlorinated organics," *J. Hazard. Mater.*, vol. 41, no. 1, pp. 73–93, 1995.

[29] D. B. Ward, C. Tizaoui, and M. J. Slater, "Ozone-Loaded Solvents for use in Water Treatment," *Ozone Sci. Eng.*, vol. 25, no. 6, pp. 485–495, 2003.
[30] B. Eliasson and U. Kogelschatz, "Nonequilibrium volume plasma chemical processing," *IEEE Trans. Plasma Sci.*, vol. 19, no. 6, pp. 1063–1077, 1991.
[31] R. Atkinson *et al.*, "Evaluated kinetic and photochemical data for atmospheric chemistry: Part 1 - gas phase reactions of Ox, HOx, NOx and SOx species," *Atmos. Chem. Phys. Discuss.*, vol. 3, no. 6, pp. 6179–6699, 2003.
[32] J. E. Gauthier and R. Snelling, "La photolyse de l' ozone a 253.7 nm: Desactivation de O(1) et de O2(1Σ) par les gaz de l'atmosphère," *J. Photochem.*, vol. 4, pp. 27–50, 1975.
[33] U. Kogelschatz, B. Eliasson, and M. Hirth, "Ozone Generation From Oxygen And Air: Discharge Physics And Reaction Mechanisms," *Ozone Sci. Eng.*, vol. 10, no. 4, pp. 367–377, 1988.
[34] K. Schofield, "Evaluated Chemical Kinetic Rate Constants for Various Gas Phase Reactions," *J. Phys. Chem. Ref. Data*, vol. 2, no. 1, pp. 25–84, 1973.
[35] R. Atkinson *et al.*, "Evaluated kinetic and photochemical for atmospheric chemistry, Organic Species: Supplement VII, IUPAC Subcommittee on Gas Kinetic Data Evaluation for Atmospheric Chemistry," *J. Phys. Chem. Ref. Data*, vol. 28, no. 2, pp. 191–393, 1999.
[36] P. Mesquida and A. Stemmer, "Guiding self-assembly with the tip of an atomic force microscope," *Scanning*, vol. 24, no. 3, pp. 117–120, 2002.
[37] R. Boukherroub, J. T. C. Wojtyk, D. D. M. Wayner, and D. J. Lockwood, "Thermal Hydrosilylation of Undecylenic Acid with Porous Silicon," *J. Electrochem. Soc.*, vol. 149, no. 2, p. H59, 2002.
[38] A. V Moshnyaga, A. V Khoroshilov, D. I. Selivanova, and D. M. Aksenova, "Thermodynamics of Dissolved Nitrogen , Nitrous Oxide , and Ammonia in Perfluorodecalin," vol. 91, no. 11, pp. 2117–2120, 2017.
[39] Y. H. Im, Z. Xiong, D. T. Elg, and D. B. Graves, "Uptake and diffusion of plasma-generated reactive nitrogen species through keratinized membrane," *J. Phys. D. Appl. Phys.*, vol. 51, no. 19, 2019.